

Estimation of Urban Greenhouse Gas Fluxes from Mole Fraction Measurements Using Monin–Obukhov Similarity Theory[©]

HELEN C. KENION^{©,d},^a KENNETH J. DAVIS,^{a,b} NATASHA L. MILES,^a VANESSA C. MONTEIRO,^{c,d}
SCOTT J. RICHARDSON,^a AND JASON P. HORNE^a

^a Department of Meteorology, The Pennsylvania State University, University Park, Pennsylvania

^b Earth and Environmental Systems Institute, The Pennsylvania State University, University Park, Pennsylvania

^c GNS Science, Lower Hutt, New Zealand

^d Antarctic Research Centre, Victoria University of Wellington, Wellington, New Zealand

(Manuscript received 13 December 2023, in final form 22 April 2024, accepted 2 July 2024)

ABSTRACT: The purpose of this study is to determine whether urban greenhouse gas (GHG) fluxes can be quantified from tower-based mole fraction measurements using Monin–Obukhov similarity theory (MOST). Tower-based GHG mole fraction networks are used in many cities to quantify whole-city GHG emissions. Local-scale, micrometeorological flux estimates would complement whole-city estimates from atmospheric inversions. CO₂ mole fraction and eddy-covariance flux data at an urban site in Indianapolis, Indiana, from October 2020 through January 2022 are analyzed. Using MOST flux-variance and flux-gradient relationships, CO₂ fluxes were calculated using these mole fraction data and compared to the eddy-covariance fluxes. MOST-based fluxes were calculated using varying measurement heights and methods of estimating stability. The MOST flux-variance relationship method showed good temporal correlation with eddy-covariance fluxes at this site but overestimated flux magnitudes. Fluxes calculated using flux-gradient relationships showed lower temporal correlation with eddy-covariance fluxes but closer magnitudes to eddy-covariance fluxes. Measurement heights closer to ground level produce more precise flux estimates for both MOST-based methods. For flux-gradient methods, flux estimates are more accurate and precise when low-altitude measurements are combined with a large vertical separation between measurement heights. When stability estimates based on eddy-covariance flux measurements are replaced with stability estimates based on the weather station or net radiation data, the MOST-based fluxes still capture the temporal patterns measured via eddy covariance. Based on these results, MOST can be used to estimate the temporal patterns in local GHG fluxes at mole fraction tower sites, complementing the small number of eddy-covariance flux measurements available in urban settings.

KEYWORDS: Atmosphere; Boundary layer; Greenhouse gases; Surface fluxes; Atmosphere-land interaction; Urban meteorology

1. Introduction

In recent years, policymakers have been taking steps toward regulation of greenhouse gas (GHG) emissions to limit the increase in global average temperature as advised by the Intergovernmental Panel on Climate Change (Pörtner and Roberts 2022; UNFCCC 2022). Urban areas must play an important role in this emissions reduction effort because they account for over 70% of GHG emissions (Birol et al. 2008). To effectively plan emissions reduction efforts, information about sources and quantities of emissions must be understood. Policymakers typically rely on emission inventories, which are activity-based estimates of GHG emissions often based on regional fuel consumption data that may be spatially disaggregated based on human activity data such as power plant locations or traffic data (Gurney et al. 2012). However, inventories for cities can take years to develop and have been shown to have large differences in estimated emissions when

compared to one another (Gately and Hutyra 2017; Gurney et al. 2021). Atmospheric approaches, such as inversions, are thus essential to improve and evaluate inventory methods. Inversions require the use of atmospheric GHG measurements at multiple locations combined with atmospheric transport models to estimate the GHG emissions over an entire region, such as a city (Lauvaux et al. 2020; Staufer et al. 2016). Lauvaux et al. (2020) found that whole-city, multimonth inverse flux estimates from Indianapolis, Indiana, had low uncertainty, but uncertainty was considerably greater for high spatial and temporal resolution emissions estimates, which are essential for process attribution.

Like inversions, eddy covariance (EC) is an effective method to estimate GHG emissions. EC measures the GHG flux directly and has a smaller footprint, measuring emissions within a distance on the order of tens to hundreds of meters from the measurement (Kljun et al. 2015). This method enables high-resolution evaluation of inventory estimates (Wu et al. 2022). EC and similar atmospheric measurements are easily computed when detecting changes in emissions, making it easier to monitor emissions in real time. This rapid response further enables the development of process-based understanding of emissions, including the evaluation of emissions mitigation measures. However, urban eddy-covariance measurements are relatively rare, and it currently is not realistic to have

[©] Supplemental information related to this paper is available at the Journals Online website: <https://doi.org/10.1175/JTECH-D-23-0164.s1>.

Corresponding author: Helen Kenion, hck5061@psu.edu

a high density of EC instruments in a city due to cost limitations.

A potential alternative method for estimating fluxes at a small spatial scale using mole fraction measurements is the use of Monin–Obukhov similarity theory (MOST). MOST relates surface fluxes to atmospheric variables including mole fraction vertical gradients and variances, as a function of atmospheric stability (Monin and Obukhov 1954). Theoretically, given the mole fraction vertical gradient or variance of a passive tracer [such as carbon dioxide (CO_2)] and the atmospheric stability, one can solve for the flux of the passive tracer. The footprint of fluxes calculated from vertical mole fraction gradients is similar to that of EC fluxes (Horst 1999), and while variance footprints have not been evaluated, they should have similar characteristics to EC since the variances in mole fraction that are critical to both measurements are the same.

There is evidence that the applicability of MOST varies site by site, particularly within the roughness sublayer. MOST was developed for the surface layer above the roughness sublayer and assumes a horizontally homogeneous surface (Foken 2006), which may not match urban conditions. Despite these limitations, MOST has been evaluated in the urban boundary layer and shown to be applicable to estimate fluxes, profiles, or variances (Pelliccioni et al. 2012; Wood et al. 2010), potentially with some site dependence in MOST functions (Dallman et al. 2013). However, such tests have typically focused on high-altitude measurements, far enough away from the surface to avoid interference from roughness elements. In practice, it is not always practical to place instruments hundreds of meters above the surface in urban areas or validate that the inlet height is outside of the roughness sublayer. MOST has been tested at lower altitudes within the roughness sublayer over forest canopies with mixed results (Katul et al. 1996; Simpson et al. 1998; Denmead and Bradley 1985). Further evaluation of MOST at lower altitudes in urban areas would be useful to test the applicability of this method in more typical urban greenhouse gas monitoring site conditions.

Adding MOST methods at urban networks would allow for smaller-scale emissions estimates surrounding mole fraction monitoring towers, which could be used to further disaggregate inversion estimates and provide more immediate emissions information in the flux footprint of these towers. Many urban emissions monitoring networks consist of sites with gas analyzers that measure GHG mole fractions rather than fluxes (Monteiro et al. 2022). If these mole fraction data could be used to estimate GHG fluxes on a site-by-site basis, emissions estimates could be made at several existing mole fraction monitoring stations. Monteiro et al. (2022) showed that networks that consist of such stations can detect abrupt changes in emissions but did not quantify the changes in emissions. Local mole fraction-based emissions estimates could be particularly useful when combined with high-density networks of low-cost instrumentation (Shusterman et al. 2016) to provide high-resolution emissions information. Such networks have already been shown to be effective in detecting and quantifying abrupt changes in emissions using inverse methods. Turner et al. (2020), for example, quantified changes in emissions due to COVID-related impacts at 900-m spatial resolution using

changes in the daily amplitude of atmospheric CO_2 from a low-altitude, low-cost sensor network.

This study aims to evaluate the use of MOST to estimate GHG fluxes from mole fraction measurements in an urban environment. The ability of this method to estimate the magnitude and temporal variability of fluxes is evaluated using EC flux measurements. If successful, MOST could be used to detect and quantify changes in emissions in time at neighborhood-scale spatial resolution. This method would make emissions estimates at such scales more accessible because it only requires one mole fraction measurement site for each flux estimate, does not require EC instrumentation, and could potentially be used with low-cost sensors. It would also allow for quick detection of temporal variation in emissions at a higher spatial resolution. This fast response is helpful in identifying specific emissions sources and monitoring how urban emissions respond to mitigation strategies.

2. Data and methods

a. Measurement site and instrumentation

All observations were collected on a communication tower in downtown Indianapolis. The tower, located at 39.7833°N , 86.1652°W , is referred to as tower 3 in the Indianapolis Flux Experiment (INFLUX) GHG monitoring network (Miles et al. 2017b). The tower is located between highway interchanges, as shown in Fig. 1, near city roads and buildings. USGS digital elevation models (USGS 2016) show that the tower is located on a hill approximately 10 m tall and 200 m wide.

EC fluxes were computed using data from a three-dimensional sonic anemometer (Campbell Scientific, Inc., model CSAT-3) and an open-path $\text{CO}_2/\text{H}_2\text{O}$ gas analyzer (LI-COR, Inc., model LI7500) mounted at 43 m above ground level (AGL). The data used in this analysis include half-hour resolution fluxes and average mole fractions measured from 7 October 2020 through 4 February 2022 (Davis 2023). The LI-COR gas analyzer and CSAT-3 sonic anemometer record data at a frequency of 10 Hz. The sonic anemometer and LI-COR gas analyzer provided EC measurements that were processed using EddyPro software (Fratini and Mauder 2014; LI-COR Biosciences 2021). We applied a block-averaging detrending method (Foken 2008; Moncreiff et al. 2004) and planar fit coordinate rotation to each half hour (Wilczak et al. 2001; Lee et al. 2004; Paw U et al. 2000). Resulting fluxes were quality controlled following steps outlined by Vickers and Mahrt (1997) for despiking, amplitude resolution, dropouts, absolute limits, discontinuities, and stationarity filtering. Friction velocity filtering was done for CO_2 fluxes (Goulden et al. 1996), separately from the friction velocity filtering in the published dataset (Davis 2023). Additionally, steps outlined by Foken and Wichura (1996) were used to evaluate stationarity, integral turbulence characteristics, and the horizontal inflow sector for each half hour, and data flags exceeding 5 based on Foken (2008) were removed.

CO_2 mole fraction measurements (Miles et al. 2017b) were collected using a wavelength-scanned cavity ring down spectroscopic instrument (Picarro, Inc., model G2301) at a frequency

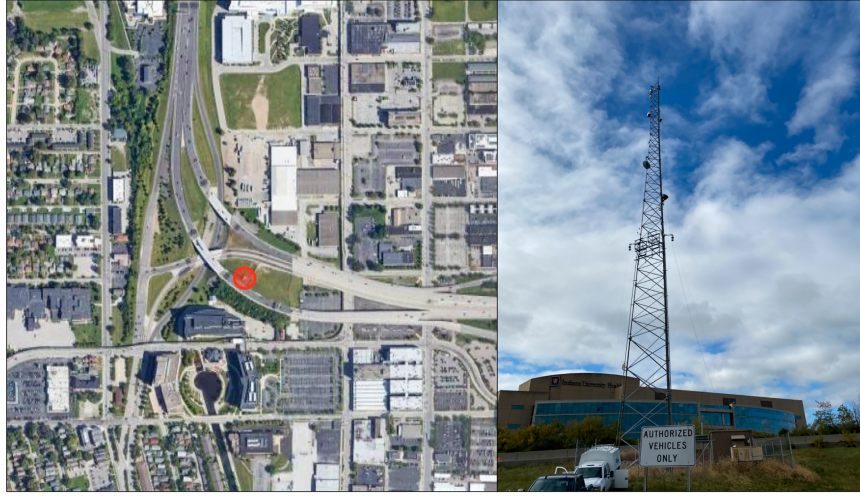


FIG. 1. (left) Satellite image of site 3 surroundings. The site location is indicated by a red star. Image from Google Maps. (right) Photo of site 3 (personal archive).

of about 0.4 Hz at inlet heights of 20, 30, 50, and 64 m AGL. Because the tower is located on top of a hill approximately 10 m high, the measurement height above ground (z_{AGL}) is effectively 10 m higher than the altitude of the measurement on the tower (z_{Tower}). Measurements are referenced as z_{AGL} in the body of the paper, where $z_{AGL} = z_{Tower} + 10$ m, and z_{AGL} is used in the flux calculations. Each hour, the top level was sampled for 30 min, with each of the lower levels sampled for 10 min using solenoid valves. Further details of the instrumentation and compatibility are described by Richardson et al. (2017) and Miles et al. (2017a).

b. Flux estimates using flux-gradient and flux-variance relationships

MOST flux-gradient and flux-variance relationships were used to estimate the CO₂ fluxes using mole fraction measurements. The MOST flux-variance relationship for a scalar, rearranged to solve for flux, is

$$|-(\bar{w}'c')_0| = \frac{\sigma_c u_*}{\phi_\theta} \quad (1)$$

(Kaimal and Finnigan 1994), where c represents the scalar mole fraction, in this case, CO₂ mole fraction. Overbars represent time-averaged means and primes represent deviations from the mean. Here, w represents the vertical wind speed, u_* is the friction velocity, σ_c is the standard deviation of the CO₂ mole fraction, $(\bar{w}'c')_0$ is the surface scalar flux, and ϕ_θ is a universal function of stability. The ϕ_θ formulation,

$$\phi_\theta = \begin{cases} 2\left(1 + 1.5\left|\frac{z}{L}\right|\right)^{-1/3}, & -2 \leq \frac{z}{L} \leq 0 \\ 2\left(1 + 0.5\frac{z}{L}\right)^{-1}, & 0 \leq \frac{z}{L} \leq 1 \end{cases} \quad (2)$$

(Kaimal and Finnigan 1994), is a function of z/L , where z is the measurement height and L is the Obukhov length. While

ϕ_θ was developed for potential temperature, it is assumed to apply to all scalars (Kaimal and Finnigan 1994). Data for which z/L was outside of these ranges were ignored.

The flux-variance relationship can be used to solve for the magnitude of the scalar flux but not its sign. Because this relationship is being applied in an urban area surrounded by CO₂ sources with little vegetation, it is assumed that the flux will be positive, which allows for the unambiguous use of the flux-variance relationship. Less than 2% of the postquality control measured EC fluxes at site 3 are negative. The MOST flux-gradient relationship (Kaimal and Finnigan 1994; Dyer 1974) rearranged to solve for scalar flux is

$$-(\bar{w}'c')_0 = \frac{kzu_* d\bar{c}}{\phi_h dz}, \quad (3)$$

where k is the von Kármán constant; z is the measurement height; $d\bar{c}/dz$ is the vertical gradient of the mean scalar, which in this case is CO₂ mole fraction; and ϕ_h is a universal function of stability. Like ϕ_θ , ϕ_h is a function of z/L assumed to apply to all scalars:

$$\phi_h = \begin{cases} 0.95\left(1 - 11.6\left|\frac{z}{L}\right|\right)^{-1/2}, & -2 \leq \frac{z}{L} \leq 0 \\ \left(0.95 + 7.8\frac{z}{L}\right), & 0 \leq \frac{z}{L} \leq 1 \end{cases} \quad (4)$$

(Högström 1988; Foken 2006). Equation (3) is integrated from the lower measurement height z_1 , to the upper height z_2 , resulting in

$$\bar{c}(z_2) = \bar{c}_{z_1} + \frac{(\bar{w}'c')_0}{ku_*} \left[0.95 \ln\left(\frac{z_2}{z_1}\right) - \psi_h\left(\frac{z_2}{L}\right) \right], \quad (5)$$

$$\psi_h = \begin{cases} 0.95 \left[2 \ln\left(\frac{1 + x_2^2}{1 + x_1^2}\right) \right], & -2 \leq \frac{z_2}{L} \leq 0 \\ -\frac{7.8}{L}(z_2 - z_1), & 0 \leq \frac{z_2}{L} \leq 1 \end{cases}, \quad (6)$$

where $x = (1 - \gamma z/L)^{1/4}$, $\gamma = 11.6$ (Högström 1988; Paulson 1970; Kaimal and Finnigan 1994), which can be used to solve for the scalar flux based on a measurement of the scalar mean mole fraction at two measurement heights.

For fluxes calculated using MOST flux-variance and flux-gradient relationships, several different flux estimates were calculated using the available mole fraction measurement heights. For variance-based MOST flux estimates, four different flux estimates were calculated at four different mole fraction measurement heights, including 20, 30, 50, and 64 m AGL. For gradient-based MOST flux estimates, this means six different flux estimates at six different combinations of two mole fraction measurement heights, combining the 20-m measurement with each of the three inlet heights above (20/30, 20/50, and 20/64 m AGL), the two middle measurement heights (30/50 m AGL), and the two upper measurement heights (50/64 m AGL). Additional flux estimates were calculated using three different stability estimation methods, which are explained in the following section. All fluxes were evaluated using the EC flux measurements at 43 m AGL.

The zero-plane displacement d is incorporated in the MOST relationships for momentum to shift what is considered the ground surface due to drag resulting from roughness elements (Garratt 1992). In the momentum equations analogous to Eqs. (1) and (3), z is replaced with $z - d$, so the distance from the measurement height to the displacement height above the ground rather than the distance to the ground surface is considered. The zero-plane displacement was not included in the MOST formulations for two reasons. First, d approaches zero when roughness elements are sparse (Garratt 1992). Roughness elements surrounding tower 3 are spread out and do not form a dense canopy. Second, while it is generally assumed that d is consistent and should be applied across all MOST relationships, it remains unclear why this would hold physically for scalar profiles (Garratt 1992), and there is not a consensus in the literature on whether it should be used in scalar relationships (Hicks et al. 1979; Raupach et al. 1979; Garratt 1979; Pelliccioni et al. 2012; Wood et al. 2010). Even so, a sensitivity analysis using 4.5 m as an upper bound for the zero-plane displacement was done to evaluate how the inclusion of the zero-plane displacement would affect the results presented in this paper and is included in the supplemental material.

c. Stability estimate

The MOST flux estimation methods were tested as an alternative to EC, so MOST fluxes were tested with and without the use of ancillary data from EC measurements. This includes the testing of three different methods of estimating the Obukhov length, one using EC data and the others without, for when EC data are not available. First, fluxes were calculated using the Obukhov length calculated using EC data. The Obukhov length is calculated using EC data collected by the sonic anemometer (Obukhov 1971; Stull 1988):

$$L = \frac{-\theta_v u_*^3}{kg(\bar{w}'\theta'_v)_0}, \quad (7)$$

where θ_v is the virtual potential temperature, u_* is the friction velocity, k is the von Kármán constant, and g is the acceleration due to gravity. This calculation was done using EddyPro (Campbell Scientific, Inc.) EC software. The L output was input directly in the MOST universal functions of z/L for the calculation of MOST fluxes. For flux estimates calculated using this stability classification method, meteorological variables including friction velocity and air density also originated from EC data output from EddyPro.

The second method for stability classification was the Grimmond and Cleugh (1994) method to determine the Obukhov lengths from net radiation data for suburban areas. The net radiation was calculated from four-component radiation data at the AmeriFlux Morgan Monroe State Forest (U.S.-MMS) site (Novick and Phillips 2022). This site is located approximately 55 km southwest of the downtown flux tower site at 39.3232°N, 86.4131°W. Instruments are mounted on a tower over a deciduous broadleaf forest, where vegetation heights are greater than 2 m and tree cover is over 60%. To estimate the Obukhov length L , net radiation data were multiplied by a daytime or nighttime constant ($\chi = 0.4$ for daytime and $\chi = 0.1$ for nighttime) that represents the ratio of sensible heat flux ($Q_h = \rho C_p \bar{w}'\theta'$, where ρC_p is the heat capacity of air at constant pressure) to net radiation (Q^*). For this method, it is assumed that the virtual potential temperature is equal to potential temperature, which in this case should differ very little. The product (χQ^*) was substituted for sensible heat flux in the equation for the Obukhov length, and $Q_h/(\rho C_p)$ was substituted for $\bar{w}'\theta'$:

$$L = \frac{-u_*^3 \rho c_p \theta}{kg Q_h} = \frac{-u_*^3 \rho c_p \theta}{kg \chi Q^*}, \quad (8)$$

where θ is the potential temperature. This L was input into the MOST universal functions of z/L for the calculation of MOST fluxes.

When this net radiation-based approach to estimate the stability was used, other variables such as friction velocity and air density were estimated using meteorological data from a nearby Automated Surface Observing System (ASOS) (NOAA 1998) rather than from the EddyPro output. This switch was made because the net radiation-based method is intended for use when eddy-covariance ancillary data are not available. The ASOS is located at the Indianapolis International Airport, approximately 14 km from the downtown flux tower site at 39.7048°N, 86.3048°W. The site surroundings include a multistory building, a managed grass lawn, and parking lots. Data from this ASOS station are obtained from the Iowa Environmental Mesonet (Iowa State University 2022). The friction velocity was calculated using the log-wind relationship (Stull 1988) using the wind speed at a measurement height of 10 m AGL at the ASOS station, with an assumed momentum roughness length of 0.1 m.

A third, alternative method was developed for estimating stability when neither EC nor net radiation data are available. This method uses a modified Pasquill stability estimate to estimate the Obukhov length using ASOS station data only. Pasquill's stability table (Pasquill and Smith 1983) was used

TABLE 1. Pasquill stability table (Davies and Singh 1985; Pasquill and Smith 1983) modified using EC stability data. Modifications include the addition of the “transition time” time of day category, which is modified slightly from the daytime category. Letters that are italicized and bolded are modifications. There are also modifications in the nighttime category, also shown in bold italics.

Surface wind speed (m s ⁻¹)	Daytime (0°–70° zenith angle) insolation			Transition time (70°–80° zenith angle) insolation			Near sunrise or sunset (80°–90° zenith angle)	Nighttime conditions	
	Strong	Moderate	Slight	Strong	Moderate	Slight		Thin overcast or >4/8 cloud	≤4/8 cloud
<2	A	A–B	B	A	B	B–C	D	E	F
2–3	A–B	B	C	B	B–C	C–D	D	D	E
3–5	B	B–C	C	B–C	C	C–D	D	D	D
5–6	C	C–D	D	C–D	D	D	D	D	D
>6	C	D	D	C–D	D	D	D	D	D

with empirical adjustments to match stability data from EC measurements. The empirical adjustments were motivated by findings from Davies and Singh (1985) that there is greater disagreement between the Pasquill stability categorization and other stability classification methods toward the beginning and end of daylight hours. Thus, a transition time category was added that differs slightly from daytime classification, for zenith angles between 70° and 80° (Table 1). These empirical adjustments to the Pasquill stability classification were made based on the same dataset that this method will be applied to, but there is no reason stability classification should differ by site. To make these adjustments, Pasquill stability classes were estimated from Obukhov lengths calculated from eddy-covariance data for each hour in the year 2021 based on Obukhov length ranges corresponding to stability classes from Golder (1972) shown in Table 2. For the same time domain and resolution, Pasquill stability classes were estimated based on cloud cover, wind speed, and solar zenith angle using ASOS station data. A comparison between the two methods of estimating stability revealed that during the transition time, the typical daytime Pasquill classification often leaned unstable compared to the Pasquill classification estimated from the Obukhov length. The transition time classification was modified accordingly from the daytime classification. Slight changes were also made to the nighttime stability classification because results showed that the nighttime Pasquill classification leaned stable.

To apply this method, Pasquill stability classes were determined from ASOS station data, and Obukhov lengths were assigned based on the range provided by Golder (1972) shown in Table 2. To determine what exact Obukhov length to assign for each range, the mean of all Obukhov lengths calculated from the eddy-covariance data corresponding to each possible Pasquill stability classification was calculated. This

mean Obukhov length, shown in Table 2, was then assigned for each hour that was assigned the corresponding Pasquill stability class. For Pasquill classifications between classes (i.e., B–C), the Obukhov length representing the boundary between the two classes from Golder (1972) was assigned (Table 2). Like for the Grimmond and Cleugh method, friction velocity and air density were calculated using ASOS station data.

d. Storage flux

EC fluxes were used for the evaluation of MOST fluxes, but EC measures the flux at the measurement height, here 43 m AGL, while the MOST methods produce the estimates of the surface flux. The EC flux should be corrected by adding the storage flux to the EC (turbulent) flux to account for the accumulation or depletion of the scalar between the surface and the measurement height (Yi et al. 2000). While EddyPro provides an estimate of CO₂ storage, it is based on a single point (LI-COR Biosciences 2015), and single-height estimates underestimate storage compared to multihight storage estimates (Saito et al. 2005). CO₂ storage was estimated using the change with time of the two lower mole fraction measurements at 20 and 30 m AGL, averaged and integrated with height following the method of Yi et al. (2000). This CO₂ storage was added to EC CO₂ fluxes prior to their comparison to MOST fluxes. As with all EC flux measurements, it was not possible to correct for systematic horizontal advection. Instead, the EC data have been filtered to remove low-turbulence conditions when horizontal advection becomes important. The typical approach of finding a u_* threshold (0.2 m s⁻¹ for this site) was used, and measurements below that threshold were discarded (Goulden et al. 1996).

TABLE 2. The inverse of the Obukhov length corresponding to each Pasquill stability class that was assigned hour-by-hour for this study, based on Golder (1972). Ranges of possible 1/L values for a given stability class from Golder (1972) are shown in the last row.

Pasquill stability class	A	A–B	B	B–C	C	C–D	D	E	F
1/L (m ⁻¹)	−0.11	−0.10	−0.066	−0.035	−0.021	−0.0072	−0.0005	0.016	0.135
Range of 1/L (m ⁻¹)	<−0.096		−0.096 < 1/L		−0.035 < 1/L		−0.0072 < 1/L	0.0070 < 1/L	1/L > 0.036

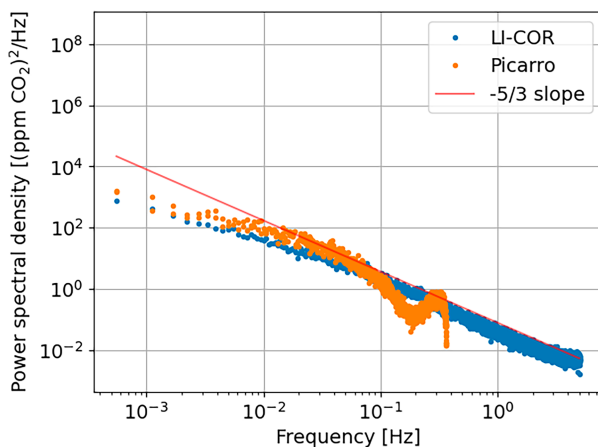


FIG. 2. Power spectral density of CO_2 mole fraction measurements from the Picarro instrument at 30 m AGL and the LI-COR at 43 m AGL, average of each half hour from 1900 UTC 16 Aug through 1600 UTC 17 Aug.

e. Spectral correction for CO_2 mole fraction variance

The measured CO_2 mole fraction variance may be affected by the type of instrument used. The frequency of the Picarro gas analyzer is about 0.4 Hz, so it does not capture any contribution to the mole fraction variance from frequencies higher than 0.4 Hz, potentially underestimating the variance. The Picarro also takes measurements through an inlet tube, in which additional mixing could take place, resulting in smoothing of measurements that would not occur with the LI-COR. This smoothing might further reduce contribution from the high-frequency measurements to the CO_2 variance (Lenshow and Raupach 1991; Berger et al. 2001). These losses can be quantified by comparing the variance to that of a higher-frequency instrument, such as the LI-COR, that measures at a frequency of 10 Hz.

The difference in the CO_2 mole fraction variance magnitude between the LI-COR and Picarro instruments was quantified by comparing their spectra. Thirty-minute spectra were computed and averaged over a 21-h period for both instruments and compared. This comparison was possible during a time period outside of the time domain used in the rest of the MOST analysis when prolonged sampling at Picarro's 30 m AGL inlet height took place, rather than the cycling through each inlet height as described in section 2a. The spectral comparison of the Picarro and LI-COR instruments confirms that the Picarro misses contributions to the variance from higher frequencies. The Picarro spectrum starts to fall from its $-5/3$ slope at a frequency of approximately 0.1 Hz (Fig. 2). To estimate the fraction of the variance the Picarro misses from the high frequencies, the ratio of the total LI-COR CO_2 variance over the variance contributed from frequencies below 0.1 Hz was calculated for each half hour and averaged, resulting in a ratio of 1.16. Because the flux-variance estimates are proportional to the square root of the variance, an increase of a factor of 1.08 in flux is expected when LI-COR rather than Picarro mole fraction data are used to calculate the flux

TABLE 3. Estimated correction factors for the CO_2 mole fraction variances calculated from Picarro data for 6- or 26-min samples. These correction factors were calculated from LI-COR CO_2 mole fraction data for the year 2021.

Stability range	Wind speed $< 3 \text{ m s}^{-1}$	Wind speed $\geq 3 \text{ m s}^{-1}$
Correction factor for 6-min sample		
$-2 < z/L < 0$	1.93	1.60
$0 < z/L < 0.1$	1.93	1.57
$0.1 < z/L < 1$	1.63	1.45
Correction factor for 26-min sample		
$-2 < z/L < 0$	1.31	1.24
$0 < z/L < 0.1$	1.42	1.26
$0.1 < z/L < 1$	1.29	1.22

estimates. The average fractional loss in variance calculated over this time period cannot, however, be universally applied over the whole dataset approximation because the scales of the eddies vary with stability and therefore time of day, so the ratio of the variances is not constant. In addition to the loss of variance in high frequencies, there is also some loss from the lower frequencies for the Picarro because in practice, variances from this instrument are calculated from 6- to 26-min samples rather than 30-min samples. This initial estimate does not consider such losses from lower frequencies.

To correct for the nonnegligible loss in variance, correction factors were estimated from spectral analysis of LI-COR CO_2 mole fraction data and applied to the Picarro variances. LI-COR raw data throughout the year 2021 were used, and for each half hour, the ratio of the total variance over the contribution of frequencies between $1/(6 \text{ min})$ and 0.4 Hz to represent inlet heights 20, 30, and 50 m that are sampled at 6-min intervals and between $1/(26 \text{ min})$ and 0.4 Hz to represent inlet height 64 m that is sampled at a 26-min interval was calculated. This simulates the ratio of the LI-COR variance over the Picarro variance because the Picarro can only capture this range of frequencies. The variance measured by the Picarro itself was not used to calculate this ratio to avoid introducing any self-correlation. These ratios were then binned by wind speed and stability to estimate correction factors that could be multiplied by the Picarro variances to correct for the loss of variance due to sampling. The correction factors are shown in Table 3. The stability and wind speed bins were chosen based on variability in the correction factors and number of data points in each category to ensure that each correction factor was estimated from a representative sample. The estimated correction factors increase with decreasing stability and are larger for lower wind speeds. Before being used to estimate fluxes, the Picarro standard deviations were multiplied by the square root of the bin-averaged variance ratios for the corresponding wind speed and stability range. It is assumed that the correction factor does not change with height, so the correction factors calculated from data at 43 m AGL are applied at all heights. In practice, correction factors may vary with height, but at this site, high-frequency instrumentation is only available at one inlet height.

f. Analyses

Average diurnal patterns of measured CO₂ mole fraction variances, vertical gradients, and EC fluxes were calculated. It is expected that the EC fluxes at the downtown flux tower site will follow traffic patterns because the footprint of the site encompasses primarily traffic sources with little vegetation. This means higher emissions during the day than at night are expected, with peaks at rush hour in the morning and late afternoon.

To determine which measurement heights and stability estimation method yield the most accurate MOST flux estimates for flux-gradient and flux-variance methods, flux temporal patterns and magnitudes were evaluated using temporal correlation coefficients and median magnitude ratios. The Spearman rank correlation coefficient for each MOST estimate with EC plus storage fluxes was calculated using hourly data for the entire dataset. The median magnitude ratio was calculated by dividing the median MOST flux over the hourly data from the entire dataset by the median EC plus storage flux. For both flux-gradient and flux-variance methods, the correlation coefficient and median magnitude ratio were calculated for each MOST measurement height or combination of measurement heights and each stability estimation method. For simplicity, only the measurement heights that produced the highest correlation coefficient with EC for MOST flux-gradient and flux-variance and the EC stability estimation method were used for the rest of the analyses. When calculating correlation coefficients between a MOST method and EC, data points from one method were dropped when the corresponding hour from the other method was missing. These data points were only dropped for the calculation of that particular correlation coefficient because dropping data points from all flux estimation methods when the corresponding hour is missing from any of the methods would result in removal of most data points.

To compare the accuracy of the flux-variance and flux gradient methods to estimate temporal patterns, the previously calculated Spearman correlation coefficients were used. Visual inspection of the data was also performed using scatterplots for both the MOST flux-gradient and the flux-variance methods compared to EC plus storage.

Potential applications of MOST flux-gradient and flux-variance methods include the estimation of long-term emissions trends, so uncertainty for each MOST flux estimation method on monthly and annual resolutions was estimated. Statistical bootstrapping was used to calculate the standard deviation of the medians over an averaging period of 30 days (Wilks 2011). For each MOST method with each stability estimation method and for the EC plus storage flux, 1000 random samples of daily averages of fluxes were taken with replacement for each sample size ranging from 1 to 365 days. The median of each random sample was calculated, and the standard deviations of the 1000 medians at each sample size was taken, producing the standard deviation of the medians. This represents the random error associated with the flux estimation method for the given sample size and will be referred to as random error in this paper. For example, the standard

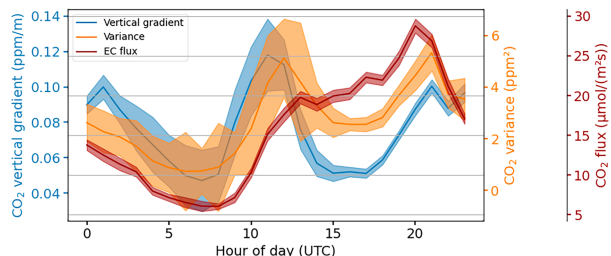


FIG. 3. Median diurnal patterns of measured CO₂ mole fraction vertical gradients, CO₂ mole fraction variances, and CO₂ flux at site 3, where the shaded region represents the standard error, from 7 Oct 2020 through 4 Feb 2022. The vertical gradient was calculated using measurements from inlet heights 64 and 20 m AGL from the Picarro. The variance, also measured by the Picarro, was measured at an inlet height of 30 m AGL. The CO₂ flux was measured by EC instrumentation at 43 m AGL and does not include storage flux.

deviation of the medians at a sample size of 30 days represents the random error for a monthly median flux estimate. This was done before comparing the magnitudes of flux-gradient and flux-variance estimates because the magnitude comparison includes a comparison of monthly medians. These uncertainty estimates include true variability in surface fluxes and thus should represent an upper bound on the random sampling error.

To evaluate the accuracy of the magnitudes and long-term trends of each flux estimation method, monthly medians and median diurnal patterns of fluxes were compared across the entire dataset. For the monthly medians, a *t* test based on the standard error of the medians calculated using bootstrapping was used to determine whether the median MOST flux estimate is significantly different from the median EC plus storage flux. Prior to the calculation of monthly median flux estimates, missing flux data were gap filled to ensure no bias by time of day when the fluxes are averaged. Gap-filled data were only used for the calculation of monthly medians, and all other analyses in this paper use data that have not been gap filled. For each month, averages of each hour of the day were taken, and for each missing data point, the average from the corresponding month and hour was used. The gap filling totaled about 13% of the data points. Weekends were removed for this analysis to isolate the higher traffic during the workweek.

3. Results

EC fluxes follow the expected diurnal pattern based on traffic data (Indiana Department of Transportation 2022) with lower nighttime fluxes, an increase in the flux in the morning, and an afternoon peak at rush hour (Fig. 3). The CO₂ mole fraction variances and gradients do not follow the same diurnal pattern as the EC flux. This is expected since the gradients and variances are functions of both the surface fluxes and atmospheric stability, and atmospheric stability is typically much greater in morning hours as compared to afternoon hours.

TABLE 4. Spearman correlation coefficients of MOST flux estimates with EC fluxes plus storage fluxes and median magnitude ratios of MOST fluxes over EC plus storage fluxes. The P values were not included because all were below 0.05, typically considered to be statistically significant.

Measurement height (m AGL)	Stability estimation method					
	EC		ASOS		Net radiation	
	Spearman r	Median magnitude ratio	Spearman r	Median magnitude ratio	Spearman r	Median magnitude ratio
MOST flux-variance estimates						
20	0.64	2.03	0.59	1.63	0.61	1.75
30	0.69	1.59	0.64	1.29	0.67	1.38
50	0.63	1.13	0.60	0.88	0.62	0.93
64	0.53	1.30	0.51	1.04	0.54	1.07
MOST flux-gradient estimates						
20 and 30	0.27	1.05	0.25	1.00	0.26	0.95
20 and 50	0.41	1.00	0.39	0.96	0.44	0.90
20 and 64	0.50	1.02	0.46	0.98	0.46	0.90
30 and 50	0.29	0.77	0.29	0.74	0.33	0.72
50 and 64	0.12	0.62	0.11	0.56	0.08	0.50

For MOST-based flux-variance inferences that use variance measurements, the highest correlation is obtained when a CO₂ mole fraction measurement height of 30 m AGL is used, true for all methods of estimating atmospheric stability. The correlation is similar when using the 20 m AGL measurement height (Table 4). There is considerable variability in median magnitude ratios between measurement heights. For the EC stability method, the median magnitude ratio for flux-variance is closest to 1 for CO₂ mole fraction variances measured at 50 m AGL, but since accurately capturing the temporal patterns of CO₂ emissions is the focus of the intended applications of this method, further MOST flux-variance results in this paper are based on the fluxes inferred from the 30 m AGL measurement height.

MOST-based flux-gradient inferences calculated using lower-altitude mole fraction measurements that also have a larger vertical separation between measurements provide the best correlation with EC fluxes and have the median magnitude ratio closest to 1. For any of the given stability estimation methods, fluxes estimated using mole fraction measurements at 64 and 20 m AGL, the highest and lowest available measurements, show a higher correlation with EC fluxes than those calculated with other measurement height combinations (Table 4). Like the flux-variance estimates, there is considerable variability in the median magnitude ratio when different inlet heights are used. Among the estimates calculated with smaller vertical separations, those with lower measurement heights have higher correlations with EC and magnitude ratios closer to 1 than those measured at higher altitudes, as evident when comparing the 64/50 m AGL estimate with the 30/20 m AGL estimate (Table 4). From this point forward, when using the MOST flux-gradient method, the results are based on the fluxes inferred from the 64 and 20 m AGL measurement heights.

For both MOST flux-variance and flux-gradient methods, there is little or no loss in temporal correlation when ASOS or net radiation stability estimation methods are used compared

to the use of the EC stability estimation method, but the magnitude ratios change. Focusing on MOST fluxes calculated using variances measured at 30 m AGL and gradients measured at 64 and 20 m AGL, the variance-based flux estimates calculated using the ASOS or net radiation stability method have lower correlation than those calculated using the EC stability method but are within 0.05 of the correlation coefficients for the EC stability method (Table 4). The median magnitude ratios are closer to 1 for the ASOS and net radiation stability methods compared to the EC stability method. The correlation coefficient for gradient-based flux estimates calculated using the alternative stability methods is lower than, but within 0.04 of, that for the estimate calculated using the EC stability method. The median magnitude ratio is further from 1 for the net radiation stability method compared to when the EC or ASOS stability method is used.

For a given stability estimation method, all MOST variance-based flux estimates showed a higher temporal correlation with EC fluxes than gradient-based estimates at an hourly time scale (Table 4). In Fig. 4, the flux-gradient estimates show more scatter, while the flux-variance estimates are more concentrated around the 1:1 line.

The random error in the monthly median and annual median flux estimates varies little between the flux estimation method and is slightly higher than the random error in EC fluxes (Table 5, Fig. 5). Alternative stability methods add little to no random error compared to the use of the Obukhov length calculated from EC data. For the flux-variance method, the random error is slightly ($\sim 1\%$) higher than the random error for the flux-gradient method. When the random error is calculated for the flux-variance method without including the spectral correction on the variance, the random error for a 30-day sample is lower and becomes closer to that of the flux-gradient method, as described in Fig. S2 in the online supplemental material.

The flux-variance method consistently overestimates the flux when compared to EC plus storage. The median magnitude

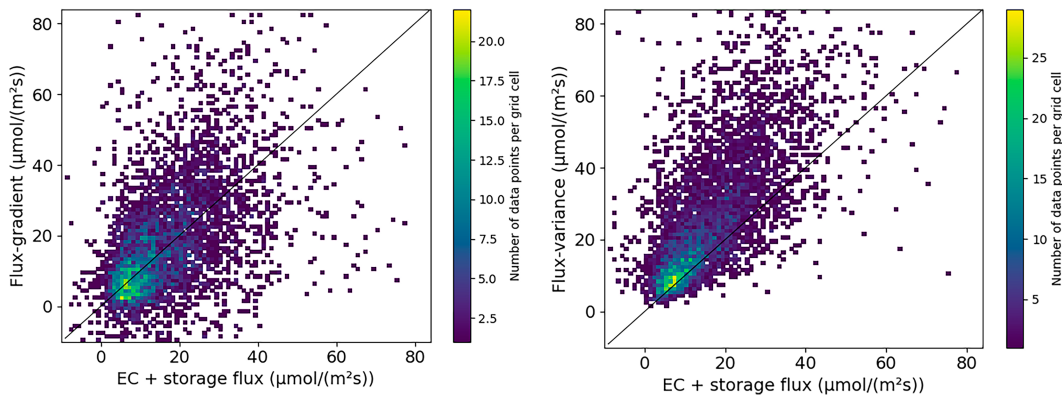


FIG. 4. Scatterplots comparing (left) MOST flux gradient estimates and (right) MOST flux–variance estimates to the EC plus storage flux. Scatterplots consist of $1 \mu\text{mol} (\text{m}^2 \text{s})^{-1} \times 1 \mu\text{mol} (\text{m}^2 \text{s})^{-1}$ grids shaded according to how many points lie within each cell. Cells that contain zero data points are white. Some grid cells containing data points are outside the range of this plot. MOST flux–variance estimates were calculated using the variance measured at 30 m AGL by the Picarro, and MOST flux–gradient estimates were calculated using mole fraction measurements from the Picarro at 64 and 20 m AGL. The Obukhov length was calculated using EC data. The black lines are 1:1 lines.

ratio is greater than the one for the flux–variance method compared to EC plus storage (Table 4). The method overestimates fluxes at all times of day, but the overestimation is larger during daytime than at night (Fig. 6). The flux–variance estimates have consistently higher monthly median fluxes than EC (Fig. 7). When the monthly median fluxes are divided by the median magnitude ratio, only August and October 2021 show a significant difference between the flux–variance estimate and the eddy-covariance flux at a 95% confidence level (Fig. S3). This suggests that, although the magnitudes do not match, the overall temporal patterns do not differ significantly except for 2 months.

The flux–gradient method does not show a clear bias in magnitude like the flux–variance method. Median flux–gradient estimates do not consistently over or underestimate the flux when compared to EC plus storage in the long-term record (Fig. 7), but the overall median flux–gradient estimate is slightly lower than that of the EC plus storage fluxes (Table 4). The diurnal pattern shows that the flux–gradient method overestimates fluxes in the afternoon (Fig. 6). While the flux–gradient monthly medians are close in magnitude to the EC medians (Fig. 7), 10 of the 15 monthly medians are significantly different

from the EC medians at a 95% confidence level (November 2020–January 2021; May–July and October–December 2021; January 2022).

4. Discussion

The diel patterns in the CO_2 mole fraction variances and vertical gradients show an intermediate step in the MOST flux estimation process before the stability estimation is included, demonstrating that the variances and vertical gradients alone do not show the same pattern as the flux. The metrics shown, vertical gradient and variance, were among the metrics Monteiro et al. (2022) used to detect, but not quantify, changes in CO_2 emissions. Figure 3, compared to the diurnal patterns of the MOST fluxes shown in Fig. 6, highlights the importance of including the stability of the atmosphere in the relationship between these metrics and the CO_2 surface flux.

Variability in flux estimates depending on the measurement height could be explained by footprint size and signal-to-noise ratio. The higher hourly correlation of flux–variance estimates with EC at a 30 m AGL measurement height could be

TABLE 5. Standard deviation of the medians for sample sizes of 30 and 365 days of daily averaged flux estimates for each flux estimation method. The standard deviation of the medians' percentage of the median EC plus storage flux over the entire dataset (October 2020–January 2022) is also shown.

Flux estimation method	Stability estimation method	Std dev of the median [$\mu\text{mol CO}_2 (\text{m}^2 \text{s})^{-1}$]			
		30-day sample	365-day sample	30-day sample	365-day sample
MOST flux–variance (30 m AGL)	EC	0.71	5.1%	0.20	1.4%
	Net radiation	0.61	4.4%	0.17	1.2%
	ASOS	0.61	4.4%	0.17	1.2%
MOST flux–gradient (64/20 m AGL)	EC	0.56	4.0%	0.18	1.3%
	Net radiation	0.58	4.1%	0.17	1.2%
	ASOS	0.60	4.3%	0.17	1.2%
EC	—	0.44	3.2%	0.13	0.95%

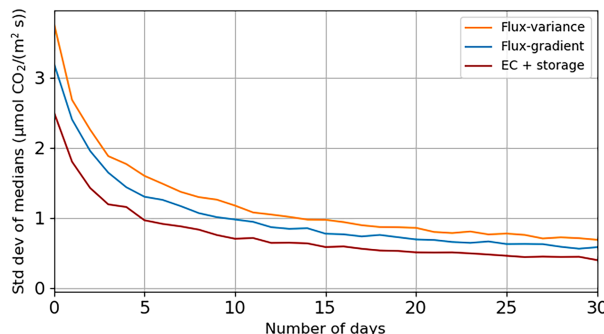


FIG. 5. Estimated random error of a sample for each sample size (number of days, x axis) of daily averaged residual flux estimates for each flux estimation method. Obukhov lengths were calculated using EC data. The flux-gradient mole fraction measurement heights are 20 and 64 m AGL, and the flux-variance mole fraction measurement height is 30 m AGL, and all mole fraction data are from the Picarro instrument.

partially because of its lower altitude and partially because of its proximity to the EC measurement height of 43 m AGL. Measurements at similar heights should have similar flux footprints, although fluxes from CO_2 sources do not vary linearly with footprint size. The correlation between EC fluxes and MOST fluxes is lower when variances at 64 m AGL are used compared to 20 m AGL, though, despite both measurement heights being relatively far from the EC measurement, suggesting that the distance from the surface also matters. Flux estimates calculated using lower altitude measurements generally have a higher correlation to EC measurements than those calculated with higher altitude measurements. Fluxes calculated using variances at measurement heights of 20, 30, and 50 m have a similar correlation with EC fluxes compared to the 64 m AGL variance fluxes. Similarity theory suggests that the scalar variances caused by surface fluxes will decrease with increasing altitude. It could be that at increasing altitudes, variances due to sources other than surface fluxes, such as changes in concentration due to advection or diurnal evolution of the boundary layer, continue to contribute to the total variance while the signal from surface fluxes decreases. This result is consistent with Monteiro et al.'s (2022) findings that only the lowest-altitude variance at this measurement site was sensitive to the decrease in CO_2 emissions due to the COVID-19 lockdown in 2020. However, the median magnitude ratios for the flux-variance estimates do not become closer to 1 for lower altitudes or show a clear pattern associated with inlet height. For fluxes calculated using gradients, vertical gradients with a larger altitude difference between measurements having better hourly correlation with EC fluxes. This may be a result of the measurements closest together in height having the smallest signal-to-noise ratio. With a smaller difference between the heights, the mole fraction differences are smaller, and any noise source has a larger fractional impact on the flux estimate. Even with smaller vertical separations, the lower-altitude measurements yield higher correlations with EC and median magnitude ratios closer to 1, as evident when comparing the 20/30 and 64/50 m

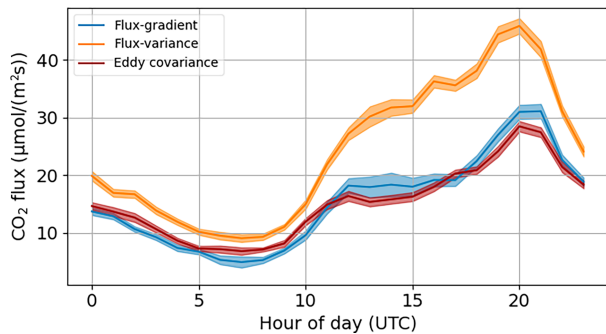


FIG. 6. Median diurnal patterns of fluxes for each hour of the day based on the entire time domain (October 2020–January 2022). These include MOST flux-variance estimates from measurements at 30 m AGL, MOST flux-gradient estimates from measurements at 64 and 20 m AGL, and EC plus storage fluxes. The shaded region represents the standard error calculated for each hour for the time domain. MOST fluxes were calculated using the EC stability data.

AGL flux-gradient estimates in Table 4. As with variances, vertical gradients in scalars caused by surface fluxes are largest at lower altitudes, so measurements at lower altitudes should be most sensitive to surface fluxes. These results are consistent with Monteiro et al.'s (2022) finding that vertical gradients are more sensitive to emissions changes when a lower height such as 20 m AGL is combined with a measurement high enough (>60 m AGL) to capture enough of the mole fraction gradient.

The minor change in temporal correlation with EC when alternative stability estimates are used depends on both how well the Obukhov length is approximated using alternative methods and data and how sensitive the estimated fluxes are to changes in the Obukhov length. The reason the median magnitude ratio would change significantly with different stability estimation methods is unclear.

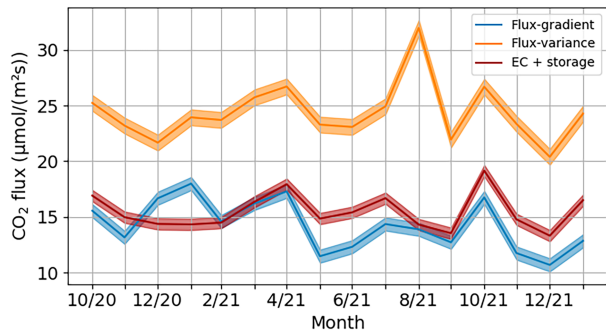


FIG. 7. Median monthly MOST flux-gradient estimates, MOST flux-variance estimates, and EC plus storage flux. Shaded regions represent 30-day standard deviation of the medians calculated using bootstrapping. MOST flux-variance estimates were calculated using the variance measured at 30 m AGL by the Picarro. MOST flux-gradient estimates were calculated using mole fraction measurements from the Picarro at 64 and 20 m AGL. The Obukhov length was calculated using EC data.

The overestimation of fluxes by the flux-variance method could be explained by surface heterogeneity. MOST and EC were developed for homogeneous surfaces. With EC, we are still able to measure surface fluxes in heterogeneous environments, but we must consider the footprint of the measurement, as discussed in a previous paragraph. It is likely that the heterogeneity of the surface fluxes impacts variances differently than covariances, however, and it would likely result in a higher CO₂ variance, even with the same area-averaged scalar surface flux. Changes in measurements with time resulting from spatial differences in flux may directly impact the variance, but possibly not the vertical gradient, because the changes with time may affect the mole fraction measurements at both vertical levels used to calculate the gradient, which depends on the difference between the two levels. If this overestimate is due to heterogeneity, it makes sense that the impact is clearest in the variance-based flux estimates and not the gradient-based estimates. The impacts of heterogeneity could be stronger during the day due to increased source heterogeneity from traffic emissions that are not present at night. This potential dependence on daytime heterogeneity would be consistent with the pattern of overestimation by the flux-variance method shown in Fig. 6. The high monthly median flux-variance estimate in August 2021 (Fig. 7) could be a result of changes in the flux footprint that include more heterogeneity for those months. This could also explain the variability of median magnitude ratios between inlet heights in the flux-variance estimates because different heights would result in different footprints with varying heterogeneity. The heterogeneity would not vary linearly with altitude.

The slight underestimation by the flux-gradient method compared to EC in the overall medians is consistent with the underestimation of fluxes by flux-gradient methods in other studies and could potentially be attributed to roughness effects. Previous studies have found underestimation of fluxes using the flux-gradient method within the roughness sublayer above forest canopies (Simpson et al. 1998), but such underestimation was larger in magnitude than in this study. The roughness elements at tower 3 also do not have a clear canopy, and there is no indication that these measurements were taken within the roughness sublayer.

MOST flux-variance methods demonstrated a higher temporal correlation with EC than flux-gradient methods, suggesting that flux-variance methods are more sensitive to changes in CO₂ emissions than flux-gradient methods. This is consistent with Monteiro et al.'s (2022) results, where statistically significant changes in emissions could be detected more often in CO₂ mole fraction variances than CO₂ vertical gradients. Lower random error for a 30-day sample for the flux-variance method when the spectral correction is not used suggests that the difference in random error associated with the flux-variance method compared to the flux-gradient method comes from the spectral correction to the standard deviations rather than the flux estimation method itself. This implies that, if a spectral correction was not needed (i.e., a higher-frequency instrument was used) or if a higher-precision spectral correction was used, the flux-variance method would

result in random noise similar in magnitude to that of the flux-gradient method.

5. Conclusions

The MOST flux-variance and flux-gradient methods have proven useful in capturing temporal patterns in local-scale CO₂ emissions. Both methods were able to capture temporal patterns in the daily cycle of emissions and have relatively high temporal correlation with eddy covariance on an hourly time scale. These methods have sufficient precision to detect relatively small month-to-month and year-to-year changes in emissions. The random error calculated in this study can be used for future work estimating monthly averaged fluxes using these methods. This random error indicates that month-to-month changes of approximately 4%–5% and year-to-year changes of approximately 1% can be detected using these methods. For example, in 2020, the City of Indianapolis Office of Sustainability reported an anticipated 27% reduction in the city's building emissions by 2025 due to a new initiative ([City of Indianapolis Office of Sustainability 2020](#)), meaning an average annual decrease of 5.4%. The random error in both the flux-variance and flux-gradient methods at 365 days is low enough to detect this change using any stability estimation method (Table 5), meaning that it will also have sufficient precision to detect a year-to-year change at this magnitude. This level of precision also exceeds INFLUX's scientific objective to quantify GHG sources with 10% or better precision, and the hourly temporal resolution meets INFLUX's goal to achieve weekly or finer temporal resolution (Davis et al. 2017). This local-scale flux estimation method can also be combined with larger-scale emissions estimation methods to improve the spatial resolution of GHG emissions estimates toward INFLUX's goal of source quantification at 1-km² resolution.

The results from this study guide the choice of measurement heights for future flux estimation using MOST methods. Measurement heights closer to ground level produce more precise flux estimates for both MOST-based methods. For MOST flux-gradient methods, flux estimates are more accurate and precise when low-altitude measurements are combined with a large vertical separation between measurement heights.

These results imply that net radiation or ASOS station data are appropriate to use as an alternative to approximate Obukhov length when measured fluxes are not available. The use of net radiation or ASOS station data to estimate atmospheric stability leads to relatively little to no degradation in the precision and accuracy of flux estimates compared to the use of eddy-covariance stability data. The loss in precision when alternative stability methods are used, if there is any, does not exceed 1%. The change in the median magnitude ratio compared to fluxes estimated using ancillary data from EC systems is substantial, though, and may need to be considered when applying these alternative methods.

This site does not meet the assumptions on which MOST is based because of the surface heterogeneity. It is likely that the magnitude of the overestimation of fluxes found here in the variance-based method would differ at sites with varying

heterogeneity. Other factors, such as stability estimation methods or measurement heights, would likely not be as affected by such a change. An area of future research would be to quantify the impact of heterogeneity on the MOST flux-variance relationship and see whether there is a dependence on source heterogeneity that could support a flux-variance formulation that includes heterogeneity.

The results from the flux-variance estimates suggest that at a given site and inlet height, monthly median estimates could be divided by a constant value to correct for overestimation. While the magnitude of overestimation by the flux-variance method varies by time of day, the overestimation is consistent over all monthly median flux estimates except for one outlier. Because the magnitude of overestimation may vary by site, the median magnitude ratio of flux-variance estimates to eddy-covariance fluxes from this site might not apply to other sites. The median magnitude ratio of the flux-gradient estimates to the eddy-covariance flux is closer to 1. The gradient-based flux magnitudes may be more robust across sites.

For future applications of MOST methods to estimate fluxes, a combination of flux-gradient and flux-variance methods would be most effective. Because the flux-variance method has better precision and temporal correlation with EC, it is best suited for the evaluation of temporal patterns, while the flux-gradient method can be used to estimate the magnitude of fluxes. For an environment such as the one studied here where CO₂ fluxes are almost always positive, the sign of fluxes is not a major concern; however, a combination of flux-variance and flux-gradient methods could potentially be used to take advantage of the good temporal precision of flux-variance estimates and the ability of the flux-gradient method to distinguish the sign.

It would also be useful to test the reliability of this method when low-cost, low-precision sensors are used for mole fraction measurements. If this method could be applied using such instrumentation, local-scale GHG flux estimation could be obtained at a higher spatial density, providing high-resolution information on temporal changes in emissions. This information could be used to disaggregate larger-scale emissions estimates such as the information typically gleaned from atmospheric inversions (e.g., Lauvaux et al. 2020) or aircraft mass-balance estimates (Heimbürger et al. 2017). Combining the MOST methods with inverse methods could improve our ability to estimate whole-city emissions while also estimating within-city temporal and spatial variability in emissions.

Acknowledgments. This work was supported by the National Oceanic and Atmospheric Administration's (NOAA) AC4 Program (Grant NA21OAR4310227 to Pennsylvania State University) and the National Institute of Standards and Technology (NIST, Grant 70NANB10H245 to Pennsylvania State University).

Data availability statement. Eddy-covariance CO₂ flux data used in this study are available at <https://doi.org/10.17190/AMF/1987603>, and CO₂ mole fraction data used in this study are available at <https://doi.org/10.18113/D37G6P>.

REFERENCES

- Berger, B. W., K. J. Davis, C. Yi, P. S. Bakwin, and C. L. Zhao, 2001: Long-term carbon dioxide fluxes from a very tall tower in a northern forest: Flux measurement methodology. *J. Atmos. Oceanic Technol.*, **18**, 529–542, [https://doi.org/10.1175/1520-0426\(2001\)018<0529:LTCDFF>2.0.CO;2](https://doi.org/10.1175/1520-0426(2001)018<0529:LTCDFF>2.0.CO;2).
- Birol, F., and Coauthors, 2008: World Energy Outlook 2008. OECD/IEA Tech. Rep., 578 pp., <https://iea.blob.core.windows.net/assets/89d1f68c-f4bf-4597-805f-901cfa6ce889/weo2008.pdf>.
- City of Indianapolis Office of Sustainability, 2020: THRIVE Indianapolis Annual Report. Tech. Doc., 16 pp., <https://static1.squarespace.com/static/5fd7a2f03c3ad531f41de6bb/t/6116c5bf12afcda1fb5b9ab8/1628882370754/FinalThriveAnnualUpdate2020+%281%29.pdf>.
- Dallman, A., S. Di Sabatino, and H. J. S. Fernando, 2013: Flow and turbulence in an industrial/suburban roughness canopy. *Environ. Fluid Mech.*, **13**, 279–307, <https://doi.org/10.1007/s10652-013-9274-7>.
- Davies, M. E., and S. Singh, 1985: Thorney Island: Its geography and meteorology. *J. Hazard. Mater.*, **11**, 91–124, [https://doi.org/10.1016/0304-3894\(85\)85034-2](https://doi.org/10.1016/0304-3894(85)85034-2).
- Davis, K. J., 2023: AmeriFlux BASE US-INC INFLUX – Downtown Indianapolis (Site-3), Ver. 2-5, AmeriFlux AMP, accessed 10 May 2023, <https://doi.org/10.17190/AMF/1987603>.
- , and Coauthors, 2017: The Indianapolis Flux Experiment (INFLUX): A test-bed for developing urban greenhouse gas emission measurements. *Elementa*, **5**, 21, <https://doi.org/10.1525/elementa.188>.
- Denmead, O. T., and E. F. Bradley, 1985: Flux-gradient relationships in a forest canopy. *The Forest-Atmosphere Interaction*, B. A. Hutchison and B. B. Hicks, Eds., Springer, 421–442.
- Dyer, A. J., 1974: A review of flux-profile relationships. *Bound.-Layer Meteor.*, **7**, 363–372, <https://doi.org/10.1007/BF00240838>.
- Foken, T., 2006: 50 years of the Monin–Obukhov similarity theory. *Bound.-Layer Meteor.*, **119**, 431–447, <https://doi.org/10.1007/s10546-006-9048-6>.
- , 2008: *Micrometeorology*. Springer, 362 pp., <https://doi.org/10.1007/978-3-642-25440-6>.
- , and B. Wichura, 1996: Tools for quality assessment of surface-based flux measurements. *Agric. For. Meteor.*, **78**, 83–105, [https://doi.org/10.1016/0168-1923\(95\)02248-1](https://doi.org/10.1016/0168-1923(95)02248-1).
- Fratini, G., and M. Mauder, 2014: Towards a consistent eddy-covariance processing: An intercomparison of EddyPro and TK3. *Atmos. Meas. Tech.*, **7**, 2273–2281, <https://doi.org/10.5194/amt-7-2273-2014>.
- Garratt, J. R., 1979: Comments on the paper ‘Analysis of flux-profile relationships above tall vegetation – An alternative view’ by B. B. Hicks, G. D. Hess and M. L. Wesely II. *Quart. J. Roy. Meteor. Soc.*, **105**, 1079–1082, <https://doi.org/10.1002/qj.49710544625>.
- , 1992: *The Atmospheric Boundary Layer*. Cambridge University Press, 316 pp.
- Gately, C. K., and L. R. Hutyra, 2017: Large uncertainties in urban-scale carbon emissions. *J. Geophys. Res. Atmos.*, **122**, 11 242–11 260, <https://doi.org/10.1002/2017JD027359>.
- Golder, D., 1972: Relations among stability parameters in the surface layer. *Bound.-Layer Meteor.*, **3**, 47–58, <https://doi.org/10.1007/BF00769106>.
- Goulden, M. L., J. W. Munger, S.-M. Fan, B. C. Daube, and S. C. Wofsy, 1996: Measurements of carbon sequestration by long-term eddy covariance: Methods and a critical evaluation of

- accuracy. *Global Change Biol.*, **2**, 169–182, <https://doi.org/10.1111/j.1365-2486.1996.tb00070.x>.
- Grimmond, C. S. B., and H. A. Cleugh, 1994: A simple method to determine Obukhov lengths for suburban areas. *J. Appl. Meteor.*, **33**, 435–440, [https://doi.org/10.1175/1520-0450\(1994\)033<0435:ASMTDO>2.0.CO;2](https://doi.org/10.1175/1520-0450(1994)033<0435:ASMTDO>2.0.CO;2).
- Gurney, K. R., I. Razlivanov, Y. Song, Y. Zhou, B. Benes, and M. Abdul-Massih, 2012: Quantification of fossil fuel CO₂ emissions on the building/street scale for a large U.S. City. *Environ. Sci. Technol.*, **46**, 12 194–12 202, <https://doi.org/10.1021/es301128z>.
- , J. Liang, G. Roest, Y. Song, K. Mueller, and T. Lauvaux, 2021: Under-reporting of greenhouse gas emissions in U.S. cities. *Nat. Commun.*, **12**, 553, <https://doi.org/10.1038/s41467-020-20871-0>.
- Heimbürger, A. M. F., and Coauthors, 2017: Assessing the optimized precision of the aircraft mass balance method for measurement of urban greenhouse gas emission rates through averaging. *Elementa*, **5**, 26, <https://doi.org/10.1525/elementa.134>.
- Hicks, B. B., G. D. Hess, and M. L. Wesely, 1979: Analysis of flux-profile relationships above tall vegetation – An alternative view. *Quart. J. Roy. Meteor. Soc.*, **105**, 1074–1077, <https://doi.org/10.1002/qj.49710544623>.
- Högström, U., 1988: Non-dimensional wind and temperature profiles in the atmospheric surface layer: A re-evaluation. *Bound.-Layer Meteor.*, **42**, 55–78, <https://doi.org/10.1007/BF00119875>.
- Horst, T. W., 1999: The footprint for estimation of atmosphere-surface exchange fluxes by profile techniques. *Bound.-Layer Meteor.*, **90**, 171–188, <https://doi.org/10.1023/A:1001774726067>.
- Indiana Department of Transportation, 2022: Traffic Count Database System (TCDS). MS2, <https://indot.public.ms2soft.com/tcds/tsearch.asp?loc=Indot&mod>.
- Iowa State University, 2022: Iowa Environmental Mesonet, IND. Iowa State University, accessed 1 May 2022, https://mesonet.agron.iastate.edu/sites/site.php?station=IND&network=IN_ASOS.
- Kaimal, J. C., and J. J. Finnigan, 1994: Flow over flat uniform terrain. *Atmospheric Boundary Layer Flows: Their Structure and Measurement*, J. C. Kaimal and J. J. Finnigan, Eds., Oxford University Press, 3–31.
- Katul, G., C.-I. Hsieh, R. Oren, D. Ellsworth, and N. Phillips, 1996: Latent and sensible heat flux predictions from a uniform pine forest using surface renewal and flux variance methods. *Bound.-Layer Meteor.*, **80**, 249–282, <https://doi.org/10.1007/BF00119545>.
- Kljun, N., P. Calanca, M. W. Rotach, and H. P. Schmid, 2015: A simple two-dimensional parameterisation for Flux Footprint Prediction (FFP). *Geosci. Model Dev.*, **8**, 3695–3713, <https://doi.org/10.5194/gmd-8-3695-2015>.
- Lauvaux, T., and Coauthors, 2020: Policy-relevant assessment of urban CO₂ emissions. *Environ. Sci. Technol.*, **54**, 10237–10245, <https://doi.org/10.1021/acs.est.0c00343>.
- Lee, X., J. Finnigan, and K. T. Paw U, 2004: Coordinate systems and flux bias error. *Handbook of Micrometeorology*, X. Lee, W. Massman, and B. Law, Eds., Springer, 33–66.
- Lenschow, D. H., and M. R. Raupach, 1991: The attenuation of fluctuations in scalar concentrations through sampling tubes. *J. Geophys. Res.*, **96**, 15 259–15 268, <https://doi.org/10.1029/91JD01437>.
- LI-COR Biosciences, 2015: EddyPro 5 instruction manual, 297 pp.
- , 2021: Eddy covariance processing software version 7.0.8. LI-COR, www.licor.com/EddyPro.
- Miles, N. L., and Coauthors, 2017a: Quantification of urban atmospheric boundary layer greenhouse gas dry mole fraction enhancements in the dormant season: Results from the Indianapolis Flux Experiment (INFLUX). *Elementa*, **5**, 27, <https://doi.org/10.1525/elementa.127>.
- , S. J. Richardson, K. J. Davis, and B. J. Haupt, 2017b: In-situ tower atmospheric measurements of carbon dioxide, methane and carbon monoxide mole fraction for the Indianapolis Flux (INFLUX) project, Indianapolis, IN, USA. Penn State Data Commons, accessed 19 December 2022, <https://doi.org/10.18113/D37G6P>.
- Moncreiff, J., R. Clement, J. Finnigan, and T. Meyers, 2004: Averaging, detrending, and filtering of eddy covariance time series. *Handbook of Micrometeorology*, X. Lee, W. Massman, and B. Law, Eds., Springer, 7–31.
- Monin, A. S., and A. M. Obukhov, 1954: Basic laws of turbulent mixing in the surface layer of the atmosphere. *Tr. Geophys. Inst. Akad. Nauk SSSR*, **24**, 163–187.
- Monteiro, V., and Coauthors, 2022: The impact of the COVID-19 lockdown on greenhouse gases: A multi-city analysis of in situ atmospheric observations. *Environ. Res. Commun.*, **4**, 041004, <https://doi.org/10.1088/2515-7620/ac66cb>.
- NOAA, 1998: Automated Surface Observing System (ASOS) user's guide. Tech. Doc. 74 pp., <https://www.weather.gov/media/asos/aum-toc.pdf>.
- Novick, K., and R. Phillips, 2022: AmeriFlux BASE US-MMS Morgan Monroe State Forest, Ver. 21-5. AmeriFlux AMP, accessed 24 August 2022, <https://doi.org/10.17190/AMF/1246080>.
- Obukhov, A. M., 1971: Turbulence in an atmosphere with a non-uniform temperature. *Bound.-Layer Meteor.*, **2**, 7–29, <https://doi.org/10.1007/BF00718085>.
- Pasquill, F., and F. B. Smith, 1983: *Atmospheric Diffusion*. 3rd ed. Ellis Horwood Limited, 437 pp.
- Paulson, C. A., 1970: The mathematical representation of wind speed and temperature profiles in the unstable atmospheric surface layer. *J. Appl. Meteor.*, **9**, 857–861, [https://doi.org/10.1175/1520-0450\(1970\)009<0857:TMROWS>2.0.CO;2](https://doi.org/10.1175/1520-0450(1970)009<0857:TMROWS>2.0.CO;2).
- Paw U, K. T., D. D. Baldocchi, T. P. Meyers, and K. B. Wilson, 2000: Correction of eddy-covariance measurements incorporating both advective effects and density fluxes. *Bound.-Layer Meteor.*, **97**, 487–511, <https://doi.org/10.1023/A:1002786702909>.
- Pelliccioni, A., P. Monti, C. Gariazzo, and G. Leuzzi, 2012: Some characteristics of the urban boundary layer above Rome, Italy, and applicability of Monin–Obukhov similarity. *Environ. Fluid Mech.*, **12**, 405–428, <https://doi.org/10.1007/s10652-012-9246-3>.
- Pörtner, H.-O., and D. C. Roberts, 2022: *Climate Change 2022: Impacts, Adaptation and Vulnerability*. IPCC, 3056 pp., <https://doi.org/10.1017/9781009325844>.
- Raupach, M. R., J. B. Stewart, and A. S. Thom, 1979: Comments on the paper ‘Analysis of flux-profile relationships above tall vegetation - an alternative view’ by B. B. Hicks, G. D. Hess and M. L. Wesely (*Q.J.*, **105**, 1074–1077) I. *Quart. J. Roy. Meteor. Soc.*, **105**, 1077–1078, <https://doi.org/10.1002/qj.49710544624>.
- Richardson, S. J., and Coauthors, 2017: Tower measurement network of in-situ CO₂, CH₄, and CO in support of the Indianapolis FLUX (INFLUX) experiment. *Elementa*, **5**, 59, <https://doi.org/10.1525/elementa.140>.
- Saito, M., A. Miyata, H. Nagai, and T. Yamada, 2005: Seasonal variation of carbon dioxide exchange in rice paddy field in Japan. *Agric. For. Meteor.*, **135**, 93–109, <https://doi.org/10.1016/j.agrformet.2005.10.007>.
- Shusterman, A. A., V. E. Teige, A. J. Turner, C. Newman, J. Kim, and R. C. Cohen, 2016: The BErkeley atmospheric CO₂

- observation network: Initial evaluation. *Atmos. Chem. Phys.*, **16**, 13 449–13 463, <https://doi.org/10.5194/acp-16-13449-2016>.
- Simpson, I. J., G. W. Thurtell, H. H. Neumann, G. Den Hartog, and G. C. Edwards, 1998: The validity of similarity theory in the roughness sublayer above forests. *Bound.-Layer Meteor.*, **87**, 69–99, <https://doi.org/10.1023/A:1000809902980>.
- Stauffer, J., and Coauthors, 2016: The first 1-year-long estimate of the Paris region fossil fuel CO₂ emissions based on atmospheric inversion. *Atmos. Chem. Phys.*, **16**, 14 703–14 726, <https://doi.org/10.5194/acp-16-14703-2016>.
- Stull, R. B., 1988: *An Introduction to Boundary Layer Meteorology*. Springer, 666 pp.
- Turner, A. J., and Coauthors, 2020: Observed impacts of COVID-19 on urban CO₂ emissions. *Geophys. Res. Lett.*, **47**, e2020GL090037, <https://doi.org/10.1029/2020GL090037>.
- UNFCCC, 2022: Report of the conference of the parties serving as the meeting of the parties to the Paris agreement on its third session, held in Glasgow from 31 October to 13 November 2021. Tech. Rep., 46 pp., <https://www.ipcc.ch/report/ar6/wg1/>.
- USGS, 2016: Digital Elevation Model (DEM) 1 meter. 3D Elevation Program, accessed 20 September 2023, <https://apps.nationalmap.gov/datasets/>.
- Vickers, D., and L. Mahrt, 1997: Quality control and flux sampling problems for tower and aircraft data. *J. Atmos. Oceanic Technol.*, **14**, 512–526, [https://doi.org/10.1175/1520-0426\(1997\)014<0512:QCACFP>2.0.CO;2](https://doi.org/10.1175/1520-0426(1997)014<0512:QCACFP>2.0.CO;2).
- Wilczak, J. M., S. P. Oncley, and S. A. Stage, 2001: Sonic anemometer tilt correction algorithms. *Bound.-Layer Meteor.*, **99**, 127–150, <https://doi.org/10.1023/A:1018966204465>.
- Wilks, D. S., 2011: *Statistical Methods in the Atmospheric Sciences*. Academic Press, 676 pp.
- Wood, C. R., and Coauthors, 2010: Turbulent flow at 190 m height above London during 2006–2008: A climatology and the applicability of similarity theory. *Bound.-Layer Meteor.*, **137**, 77–96, <https://doi.org/10.1007/s10546-010-9516-x>.
- Wu, K., and Coauthors, 2022: Source decomposition of eddy-covariance CO₂ flux measurements for evaluating a high-resolution urban CO₂ emissions inventory. *Environ. Res. Lett.*, **17**, 074035, <https://doi.org/10.1088/1748-9326/ac7c29>.
- Yi, C., K. J. Davis, P. S. Bakwin, B. W. Berger, and L. C. Marr, 2000: Influence of advection on measurements of the net ecosystem-atmosphere exchange of CO₂ from a very tall tower. *J. Geophys. Res.*, **105**, 9991–9999, <https://doi.org/10.1029/2000JD900080>.